2-2012

Tricriticality in generalized Schloegl models for autocatalysis: Lattice-gas realization with particle diffusion

Xiaofang Guo
Iowa State University, mlmayor@iastate.edu

Daniel K. Unruh
Iowa State University

Da-Jiang Liu
Ames Laboratory, dajiang@fi.ameslab.gov

James W. Evans
Iowa State University, evans@ameslab.gov

Tricriticality in generalized Schloegl models for autocatalysis: Lattice-gas realization with particle diffusion

Abstract

We analyze lattice–gas reaction–diffusion models which include spontaneous annihilation, autocatalytic creation, and diffusion of particles, and which incorporate the particle creation mechanisms of both Schloegl's first and second models. For fixed particle diffusion or hop rate, adjusting the relative strength of these creation mechanisms induces a crossover between continuous and discontinuous transitions to a "poisoned" vacuum state. Kinetic Monte Carlo simulations are performed to map out the corresponding tricritical line as a function of hop rate. An analysis is also provided of the tricritical "epidemic exponent" for the case of no hopping. The phase diagram is also recovered qualitatively by applying mean-field and pair-approximations to the exact hierarchical form of the master equation for these models.

Keywords

Schloegl's model, Contact process, Non-equilibrium phase transitions, Tricriticality

Physica A 391, 633-646 (2012).

TRICRITICALITY IN GENERALIZED SCHLOEGL MODELS FOR AUTOCATALYSIS: LATTICE-GAS REALIZATION WITH PARTICLE DIFFFUSION

Xiaofang Guo[1,2], Daniel K. Unruh[1], Da-Jiang Liu[1], and James W. Evans[1,2]

Ames Laboratory – USDOE[1] and Departments of Mathematics[2] and Physics & Astronomy[2], Iowa State University, Ames Iowa 50011

ABSTRACT

We analyze lattice-gas reaction-diffusion models which include spontaneous annihilation, autocatalytic creation, and diffusion of particles, and which incorporate the particle creation mechanisms of both Schloegl's first and second models. For fixed particle diffusion or hop rate, adjusting the relative strength of these creation mechanisms induces a crossover between continuous and discontinuous transitions to a "poisoned" vacuum state. Kinetic Monte Carlo simulations are performed to map out the corresponding tricritical line as a function of hop rate. An analysis is also provided of the tricritical "epidemic exponent" for the case of no hopping. The phase diagram is also recovered qualitatively by applying mean-field and pair-approximations to the exact hierarchical form of the master equation for these models.

PACS: 05.70.Fh, 02.50.Ey, 05.50.+q, 05.70.Ln

Key words: Schloegl's model; contact process; non-equilibrium phase transitions; tricriticality

Corresponding author: J.W. Evans, Ames Laboratory – USDOE, Iowa State University, Ames Iowa 50011; Tel: 515-294-1638; Fax: 515-294-4709; email: evans@ameslab.gov

1. INTRODUCTION

While non-equilibrium systems can display a richer variety of phase transition or bifurcation behavior than traditional equilibrium systems, there are also many similarities in behavior [1,2]. At the mean-field level of analysis, bistability of non-equilibrium steady states corresponds to van der Waals loops for equilibrated fluids. The disappearance of bistability at a cusp bifurcation is the non-equilibrium analogue of a critical point [2-4]. One can also construct non-equilibrium models which exhibit continuous phase transitions at the mean-field level.

However, a natural goal is to advance beyond mean-field-level to statistical mechanical analyses of these non-equilibrium models. Most such studies of non-equilibrium phase transitions in lattice-gas models have focused on universality in continuous transitions [5-7]. However, increasing attention is being paid to analysis of various phenomena in reaction-diffusion type models exhibiting discontinuous transitions [8-14]. It is thus also natural to explore the crossover between continuous and discontinuous transitions, i.e., to assess tricritical behavior in non-equilibrium systems [15]. We achieve this goal by analyzing a generalized version of Schloegl's first and second models for autocatalysis involving both spontaneous annihilation and autocatalytic creation of particles (denoted by X), as described below.

In traditional off-lattice mean-field formulations, Schloegl's first (n=1) and second (n=2) models include the processes [2,14,16-22]:

$X \rightarrow \varnothing$ (spontaneous annihilation), $nX \rightarrow (n+1)X$ (autocatalytic creation).

Annihilation occurs spontaneously at rate p (the control variable in the model), but autocatalytic creation requires an existing nearby particle in the first model (n=1), or a nearby pair of particles in the second model (n=2). Rates for these processes are prescribed below. Most investigations of Schloegl's models include spontaneous particle creation $\varnothing \rightarrow X$, but this process is excluded in our study. Furthermore, in traditional off-lattice formulations, it is necessary include the autocatalytic annihilation process $(n+1)X \rightarrow nX$ in order to avoid population explosion [2,16].

Particle diffusion is also usually regarded as being active. These models display quadratic (cubic) mean-field kinetics for n=1 (n=2), i.e., the rate of change of particle concentration is a quadratic (cubic) function of concentration, C [2,16-19]. Upon increasing the annihilation rate p, there is a bifurcation in the steady-states from a regime supporting an "active" or "reactive" stable steady state with finite population C>0 to one where the vacuum state (C=0) is the unique stable steady state [5,22]. For n=1, this transition is a (continuous) transcritical bifurcation, but for n=2 it is a (discontinuous) fold- or saddle-node type bifurcation.

In this work, we will consider exclusively lattice-gas formulations of Schloegl's models where autocatalytic particle creation requires an empty site $\varnothing$, and is thus more accurately represented as $nX+\varnothing\rightarrow(n+1)X$ [14,19-22]. This empty site requirement automatically limits population growth. The mean-field treatment of these models has essentially the same features as the traditional off-lattice formulation including autocatalytic annihilation. Our lattice-gas formulation of Schloegl's models corresponds to and can also be described as the standard Contact Process (SCP) for the first model (n=1), and as the Quadratic Contact Process (QCP) for the second model (n=2) [5,14,20-22]. The SCP provides the prototype for a continuous phase transition to an absorbing vacuum state, where the transition is in the universality class of directed percolation or Reggeon field theory [5]. The QCP, at least with a suitable choice of rates, provides an example of a discontinuous phase transition displaying generic two-phase coexistence [14].

Our investigation will adopt a lattice-gas realization of a generalized version of Schloegl's first and second models (or, equivalently, a hybrid QCP+SCP model) with particle hopping. Our focus is on analysis of tricritical behavior associated with the conversion between continuous and discontinuous transitions. For the most part, we focus on the regime where the QCP is perturbed by adding a "small amount" of the SCP mechanism. From this perspective, the generalized model provides additional insight into the behavior of the pure QCP, particularly for small particle hop rate where unusual generic two-phase coexistence is observed.

In Sec.2, we describe in detail a lattice-gas realization of the version of our hybrid QCP+SCP model for which tricritical behavior will be analyzed in detail. Other hybrid models displaying tricriticality are discussed in the Appendices and in Ref.[15]. In addition, we present the hierarchical form of the exact master equation for this model. Mean-field behavior is also briefly described. In Sec.3, we present simulation results focusing on determination of the tricritical point as a function of hop rate. A more detailed analysis of tricritical behavior is also provided for the case of no hopping. Next, in Sec.4, we present an analysis of model behavior within the pair-approximation to the exact master equation. This approximation describes qualitatively behavior observed in simulation studies. Conclusions are provided in Sec.5.

2. MODEL SPECIFICATION AND MASTER EQUATIONS

2A. MODEL PRESCRIPTION

Our realization the generalized Schloegl model (or hybrid QCP+SCP) as a stochastic Markov process on a square lattice involves the following steps (cf. Ref.[14,20-22]): **(i)** particle annihilation occurring randomly at rate p; **(ii)** a QCP pathway for particle creation at empty sites requiring one or more diagonally adjacent pairs of occupied sites; specifically, the creation rate is given by k/4, where k is the number of adjacent diagonal occupied pairs taking values k = 0, 1, 2, or 4; **(iii)** a SCP pathway for particle creation at empty sites requiring just one or more adjacent occupied sites; specifically, the creation rate is given by $j\cdot\delta$, where j is the number of adjacent occupied sites taking values j = 0-4; **(iv)** hopping of particles to any adjacent empty sites at rate h (per target site). **Fig.1** provides a schematic of these processes. Note that for any empty site with at least one diagonal adjacent pair of occupied sites, particles can be created by either the QCP or SCP pathway (a feature absent in the modification discussed in the Appendix). Setting $\delta=0$ recovers the QCP with particle diffusion.

Again, C will denote the particle concentration, i.e., the fraction of filled sites. For any $p>0$, the "vacuum state" with C=0 corresponds to an absorbing steady state from which the system cannot escape. However, there also exists an active or reactive steady-state with $C=C_{eq}(p)>0$, at least for small p. Indeed, for $p<<1$, the lattice is almost completely populated in

this active state, so essentially all empty sites have k=j=4. Consequently, particle creation at each empty site effectively occurs with the same rate 1+4δ, and one has that $C_{eq}(p) = 1-(1+4\delta)^{-1}p + O(p^2)$, independent of h. Kinetic Monte Carlo (KMC) simulation will be utilized below to provide precise results for $C_{eq}(p)$ versus p (i.e., the equation of state) for a broad range of p with various δ and h. For each specific hop rate h, KMC analysis that the model exhibits a discontinuous transition to a vacuum state for $\delta<\delta_{tc}(h)$, and a continuous transition for $\delta>\delta_{tc}(h)$. We can thus determine the tricritical line $\delta_{tc}=\delta_{tc}(h)$ versus h.

2B. HIERARCHICAL MASTER EQUATIONS

It is also instructive to present the exact master equation for the hybrid QCP+SCP with h≥0 in the form of an infinite coupled hierarchy. Exploration of the predictions of truncation approximations to these equations provides additional insight into model behavior.

First, we consider spatially homogeneous states of the hybrid QCP+SCP with h≥0 on an infinite square lattice. We let "x" denote an occupied site and "o" an empty site. Then, P[x] = C denotes the probability of an occupied site, P[o] = 1-C the probability of an empty site, P[x x] the probability of an adjacent occupied pair, P[o o] the probability of an adjacent empty pair, etc.. Conservation of probability ensures that all configurational probabilities can be written as combinations of such probabilities for configurations with just empty sites, e.g., P[x] = 1 - P[o], P[x o] = P[o] - P[o o], P[xx] = 1 - 2P[o] + P[o o], etc. [23]. Instead, one could favor just occupied-site configurations. For the QCP, we favor empty site configurations when developing the master equation. This facilitates substantial simplification of the equations, as illustrated below. A similar situation applies for models which just include irreversible cooperative creation of particles and no annihilation or hopping, usually referred to as "cooperative sequential adsorption" models [23]. The exact form of the first two such hierarchical master equations in an infinite coupled set becomes (cf. Ref.[24])

$$\mathrm{d/dt}\ P[o] = p\cdot P[x] - \left(4\cdot\frac{1}{4}\cdot P\begin{bmatrix} & x & \\ o & o & x \\ & o & \end{bmatrix} + 4\cdot\frac{1}{2}\cdot P\begin{bmatrix} & x & \\ o & o & x \\ & x & \end{bmatrix} + 1\cdot 1\cdot P\begin{bmatrix} & x & \\ x & o & x \\ & x & \end{bmatrix} \right)$$

$$-\delta\cdot\left(4\cdot 1\cdot P\begin{bmatrix} & o & \\ o & o & x \\ & o & \end{bmatrix} + 4\cdot 2\cdot P\begin{bmatrix} & x & \\ o & o & x \\ & o & \end{bmatrix} + 2\cdot 2\cdot P\begin{bmatrix} & o & \\ x & o & x \\ & o & \end{bmatrix} + 4\cdot 3\cdot P\begin{bmatrix} & x & \\ x & o & x \\ & o & \end{bmatrix} + 1\cdot 4\cdot P\begin{bmatrix} & x & \\ x & o & x \\ & x & \end{bmatrix} \right)$$

$$= p\cdot P[x] - P\begin{bmatrix} x & \\ o & x \end{bmatrix} - 4\delta\cdot P[o\quad x] \qquad (1)$$

$$\mathrm{d/dt}\ P[o\quad o] = 2p\cdot P[o\quad x] - 2\cdot\left(2\cdot\frac{1}{4}\cdot P\begin{bmatrix} & x & \\ o & o & x \\ & o & \end{bmatrix} + 1\cdot\frac{1}{2}\cdot P\begin{bmatrix} & x & \\ o & o & x \\ & x & \end{bmatrix} \right)$$

$$-2\delta\cdot\left(3\cdot 1\cdot P\begin{bmatrix} & o & \\ o & o & x \\ & o & \end{bmatrix} + 2\cdot 2\cdot P\begin{bmatrix} & x & \\ o & o & x \\ & o & \end{bmatrix} + 1\cdot 2\cdot P\begin{bmatrix} & x & \\ o & o & o \\ & x & \end{bmatrix} + 1\cdot 3\cdot P\begin{bmatrix} & x & \\ o & o & x \\ & x & \end{bmatrix} \right)$$

$$+2h\cdot\left(P[o\quad x\quad o] + 2\cdot P\begin{bmatrix} & o \\ o & x \end{bmatrix} - P[o\quad o\quad x] - 2\cdot P\begin{bmatrix} & x \\ o & o \end{bmatrix} \right)$$

$$= 2p\cdot P[o\quad x] - P\begin{bmatrix} & x & \\ o & o & x \end{bmatrix} - 2\delta\cdot P[o\quad o\quad x] - 4\delta\cdot P\begin{bmatrix} & x \\ o & o \end{bmatrix}$$

$$+2h\cdot\left(P[o\quad -\quad o] + 2\cdot P\begin{bmatrix} & o \\ o & - \end{bmatrix} - 3\cdot P[o\quad o] \right) \qquad (2)$$

where again probabilities of configurations involving filled sites can be rewritten in terms of those just involving empty sites. The first gain terms in (1) and (2) (proportional to p) correspond to particle annihilation. The second group of loss terms corresponds to autocatalytic creation via the QCP mechanism. The third group of loss terms (proportional to δ) corresponds to autocatalytic creation via the SCP mechanism. The last group of terms in the P[o o]-equation (proportional to h) corresponds to particle hopping. Particle hopping terms are absent in the P[o]-

equation since hopping preserves particle number. After the second equality, we have implemented an exact summation and simplification of terms associated with particle creation for both QCP and SCP mechanisms (cf. Ref. [24]). Likewise, the hopping terms incorporate an exact cancellation and simplification due to conservation of probability applicable for the special case of particle hopping with simple site exclusion (cf. Ref.s [25,26]). We have also exploited rotational symmetries to identify equivalent contributions.

One can extend the above exact hierarchy to treat spatially non-uniform states [24]. Here, one introduces the probabilities $P[x_{i,j}] = C_{i,j}$ that site (i,j) is occupied, $P[o_{i,j}] = 1-C_{i,j}$ that site (i,j) is empty, $P[o_{i,j}\, o_{i+1,j}]$ that both sites (i,j) and (i+1,j) are empty, etc.. The form of the hierarchy naturally extends (1) and (2) above [24], but now hopping terms appear in the equation for the single-site quantity of the form [26]

$$d/dt\ P[o_{i,j}]|_{hop} = h(P[o_{i+1,j}]+P[o_{i,j+1}]+P[o_{i-1,j}]+P[o_{i,j-1}]-4P[o_{i,j}]). \qquad (3)$$

2C. MEAN-FIELD BEHAVIOR

It is instructive to provide a mean-field analysis for the above QCP+SCP model. Mean-field treatments ignore all spatial correlations, so probabilities of multi-site configurations factor as a product of constituent single-site probabilities. Such a treatment describes exactly behavior in the limit $h\to\infty$ where the system is "well-stirred" by rapid particle diffusion. We apply this procedure to the spatially non-uniform version of (1), and formulate the resulting evolution in terms of a coarse-grained particle concentration, $C(\underline{r}=(i,j)a) = C_{i,j}$, which in general varies slowly on a length scale $O(a\, h^{1/2})$ as a function of a quasi-continuous position $\underline{r} = (i,j)a$. Here 'a' denotes the lattice constant. One then obtains the mean-field reaction-diffusion equation (RDE)

$$\partial C/\partial t = R(C) + D\,\nabla^2 C \text{ with } R(C) = -p\cdot C + C^2(1-C) + 4\delta\cdot C(1-C), \qquad (4)$$

and where $D=a^2 h$ denotes the particle diffusion coefficient. One finds a stable uniform active steady state satisfying $p=C(1-C)+4\delta(1-C)$ for certain p, as well as a vacuum steady-state C=0.

Mean-field steady-state behavior (i.e., the equation of state) for $h\to\infty$ is presented in **Fig.2**. When $\delta < \delta_{tc}(mf) = ¼$, the model supports a stable active state for $0 \le p \le p_{s+}(\delta)$ and a stable vacuum state for $p \ge p_{s-}(\delta)$, i.e., the model displays bistability for $p_{s-}(\delta) < p < p_{s+}(\delta)$. The upper and lower spinodals satisfy

$$p_{s-}(\delta) = 4\delta \text{ and } p_{s+}(\delta) = (1+4\delta)^2/4 = 4\delta + (1-4\delta)^2/4. \quad (5)$$

For $p<p_{s-}$ ($p>p_{s+}$), only the active (vacuum) state is stable. Bistability disappears at $\delta = \delta_{tc}(mf)$. For $\delta>\delta_{tc}(mf)$, one instead finds a continuous transition at $p=p_{cts}(\delta) = 4\delta$ from a unique stable active steady-state exists for $p<p_{cts}(\delta)$ to a unique stable vacuum state for $p>p_{cts}(\delta)$ [27].

Additional characterization of steady-state behavior comes from writing

$$R(C) = -d/dC\ U(C) \text{ with } U(C) = ½\ (p-4\delta)C^2 – 1/3\ (1-4\delta)C^3 + ¼\ C^4. \quad (6)$$

The effective free energy density, U(C), has a double-well form when $\delta < \delta_{tc}$ for $p_{s-}(\delta) < p < p_{s+}(\delta)$, and reduces to $U(C) = ¼\ C^2(2/3 -8\delta/3 -C)^2$ with equal well heights when $p = p_{eq}(\delta) = 4\delta+(2/9)(4\delta–1)^2$. Insight into the significance of $p=p_{eq}(\delta)$ comes from analysis based on the RDE (4) for the evolution of an interface separating the stable active state from the stable vacuum state in the bistable region. One finds that the interface is stationary at $p = p_{eq}(\delta)$, i.e., this corresponds to the equistability point for the active and vacuum states within the bistable region.

Fig. 3 shows the phase diagram in the p-δ plane for the mean-field QCP+SCP including the spinodal lines, $p=p_{s\pm}(\delta)$, and the equistability line, $p=p_{eq}(\delta)$, for $\delta<\delta_{tc}(mf)$ which merge at $\delta=\delta_{tc}(mf)$. The continuation of these lines for $\delta>\delta_{tc}(mf)$ is given by $p=p_{cts}(\delta)$ corresponding to the continuous transition. In a stochastic or statistical mechanical version of the model, $p_{eq}(\delta)$

would correspond to the location of a discontinuous transition. Thus, it is natural to introduce a general transition $p = p_{tr}(\delta)$ which would correspond to the discontinuous transition $p_{tr}(\delta) = p_{eq}(\delta)$ for $\delta<\delta_{tc}(mf)$ and to the continuous transition $p_{tr}(\delta) = p_{cts}(\delta)$ for $\delta>\delta_{tc}(mf)$. Then, $\delta = \delta_{tc}$ corresponds to a tricritical point.

3. SIMULATION RESULTS: TRICRITICAL BEHAVIOR IN THE QCP+SCP

As δ increases above zero in the hybrid QCP+SCP for fixed particle hop rate $h\geq 0$, one expects a conversion from a discontinuous to a continuous transition upon reaching a tricritical value $\delta=\delta_{tc}$. Our primary goal here is to apply kinetic Monte Carlo simulations to determine $\delta=\delta_{tc}$ (which depends on h). One complication is that for $\delta=0$, the (QCP) model exhibits generic two-phase coexistence: stable active and vacuum states coexist not just for a single value of annihilation rate p (as expected for a thermodynamic system), but rather for a finite range $p_f(\delta) < p < p_e(\delta)$. This behavior reflects the feature that the equistability of active and vacuum states separated by a planar interface depends on the orientation of the interface, the equistability value of $p = p_{eq}(\delta)$ for varying from $p_e(\delta)$ to $p_f(\delta)$ as the orientation changes from diagonal to horizontal (or vertical). Previous analysis for the QCP with $\delta=0$ revealed that $p_e = 0.0944$ and $p_f = 0.0869$ when h=0, but that $\Delta p_{eq} = p_e - p_f$ decreases very quickly with increasing h from $\Delta p_{eq} = 0.0075$ when h=0 to $\Delta p_{eq} < 10^{-4}$ when h=0.02. Similarly, for the QCP with fixed $h\geq 0$, we expect that generic two-phase coexistence persists for $\delta>0$, but that Δp_{eq} decreases quickly with increasing δ and vanishes at $\delta = \delta_{tc}$. New results for h=0 and increasing $\delta>0$ are shown in **Table I** confirming the very rapid decrease of Δp_{eq} with increasing δ [28].

Thus, as a practical matter, except very close to $(\delta, h)=(0, 0)$, one has that $p_{eq}(\delta) = p_e(\delta) \approx p_f(\delta)$ in the QCP+SCP for $\delta<\delta_{tc}$, corresponding to the location of a discontinuous transition $p_{tr}(\delta) = p_{eq}(\delta)$. For $\delta>\delta_{tc}$, the discontinuous transition is replaced by a continuous transition at $p = p_{tr}(\delta) = p_{cts}(\delta)$.

3A. TRANSITION LOCATION

Our initial goal for analysis of the QCP+SCP for fixed h (including h=0) and varying δ is to determine the value of $p= p_{tr}(\delta)$ at the non-equilibrium phase transition as a function of δ (where again the transition is discontinuous for $\delta<\delta_{tc}$, and continuous for $\delta>\delta_{tc}$). Rather than conventional "constant-p" simulations, it is more convenient to utilize "constant concentration" (CC) simulations [29]. In the former, one selects p and then decides whether to annihilate or create a particle at a randomly selected site based on this value. For the latter CC simulations [29], one selects a target particle concentration C_t and annihilates (creates) a particle and a randomly selected site if the actual concentration satisfies $C>C_t$ ($C<C_t$). The p-value associated with C_t is then determined from the fraction of attempts to annihilate a particle. The constant-p and the constant concentration simulations should be consistent for a large system. However, the latter are particularly convenient for determining the locations of discontinuous and continuous transitions, our initial objective here. (CC simulations are also effective for determining the regime of generic two-phase coexistence.) These simulation results also provide an estimate of the location $\delta=\delta_{tc}$ of the conversion from a discontinuous to a continuous transition.

Fig.4a presents results from CC simulations for p versus C in the QCP+SCP with h=0 for various δ>0. From these results, we extract precise estimates of the transition location $p=p_{tr}(\delta)$ versus δ>0 shown in **Table II** for h=0. In addition, analysis of this data to determine $dp/dC|_{C=0}$ versus δ reveals a sudden transition from small positive values to substantial negative values as δ exceeds a tricritical value of $\delta_{tc}(h=0) \approx 0.032$. A refined determination of $\delta_{tc}(h=0)$ will be provided immediately below. These results for $p_{tr}(\delta)$ versus δ, the estimate of $\delta_{tc}(h=0)$, and also more detailed results for $p_e(\delta)$ and $p_f(\delta)$ versus δ from **Table I** for h=0, are summarized in **Fig.4b**.

3B. EPIDEMIC ANALYSIS

For a more detailed characterization of behavior at the transition point $p=p_{tr}(\delta)$ and in particular at the tricritical point, $\delta=\delta_{tc}$, for the QCP+SCP with h=0, we perform an "epidemic

analysis" [5,9] to assess the evolution of a patch of filled sites (or a patch of the active state) embedded in the vacuum state. Of particular interest is the behavior at $p=p_{tr}(\delta)$ of survival probability, $P_s(t)$, versus t. For a continuous transition when δ exceeds δ_{tc}, one should find that that $P_s(t) \sim t^{-\zeta}$, as $t\rightarrow\infty$, where the exponent $\zeta = \zeta_{DP} \approx 0.451$ adopts the value of the directed percolation universality class [5,15]. However, exactly at the tricritical point $\zeta = \zeta_{tc}$ will adopt a distinct value $\zeta_{tc} > \zeta_{DP}$ associated with the universality class of non-equilibrium tricriticality. Furthermore, for δ just above δ_{tc}, the effective value of ζ would plausibly be controlled by ζ_{tc} rather than ζ_{DP}. For a discontinuous transition when $\delta<\delta_{tc}$, one expects that asymptotically $P_s(t)\rightarrow 0$ exponentially as $t\rightarrow\infty$ [12] unless there is a very weak effective line tension of the interface between active and vacuum states [9,10]. However, in practice, simulation data might mimic algebraic decay with a larger exponent ζ [9,10,12]. The inset to **Fig.5** shows behavior of $P_s(t)$ versus t for the QCP+SCP with h=0 at $p=p_{tr}(\delta)$ for a broad range of δ=0.01-0.07 which is consistent with the above picture.

The above observations indicate that the effective ζ will evolve from values smaller than ζ_{tc} to values larger than ζ_{tc} as δ increases through δ_{tc}. Correspondingly, the plot of $\ln[P_s(t)]$ versus $\ln[t]$ evolves from positive to negative curvature for larger $\ln[t]$ as δ increases through δ_{tc}. See the main part of **Fig.5** which shows high quality data for a restricted range of δ around δ_{tc}. With this in mind, it is natural to fit simulation data for a suitable range of t to the form

$$\ln[P_s(t)] \approx - \zeta_0 - \zeta_1 \ln[t] - \zeta_2 (\ln[t])^2. \qquad (7)$$

Then, ζ_2 should evolve from negative values for $\delta<\delta_{tc}$ to positive values for $\delta>\delta_{tc}$. Thus, the optimum estimate of δ_{tc} should come from the value of δ when $\zeta_2=0$, and the optimum estimate of ζ_{tc} should come from the value of ζ_1 at this point. Thus, the simulation data shown in **Fig.5**, and the associated ζ_1 and ζ_2 values reported in **Table III** from the range t=1000-8000 indicate that $\delta_{tc} \approx 0.0338\pm0.0010$ and $\zeta_{tc} \approx 1.23\pm0.10$ for the QCP+SCP with h=0.

Finally in this section, we briefly assess the location of the tricritical point in the QCP+SCP with finite h>0. Here, we have just performed a CC analysis for various h>0 to determine $p_{tr}(\delta)$ versus δ, and the value of $\delta=\delta_{tc}(h)$. Results for $C_{eq}(p)$ versus p with h=0.5 are shown in **Fig.6**, and an analysis of the corresponding $dp/dC|_{C=0}$ versus δ reveals a sudden transition to negative values as δ exceeds $\delta_{tc}(h=0.5) \approx 0.070$. Results for $\delta_{tc}(h)$ from a similar analysis for other finite h, together with the exact result for $h=\infty$ from the mean-field analysis in Sec.2, are plotted to show the entire tricritical line in **Fig.7**.

4. PAIR-APPROXIMATION ANALYSIS: TRICRITICAL BEHAVIOR IN THE QCP+SCP

4A. KINETICS AND STEADY-STATES

First, we consider an approximate analysis of the exact master equation for spatially uniform states. The lowest-order mean-field site-approximation (which ignores all spatial correlations) fails to capture the h-dependence of the reaction kinetics. However, this dependence which is of particular interest in this work is described by the higher-order approximations. Here, we consider only the pair-approximation [24,30]. In the hierarchical master equation for uniform states (1), this approximation factorizes multi-site probabilities in the particle creation terms as products of the m constituent pair probabilities and divides by $P[o]^{m-1}$ to avoid over-counting of the shared central empty site. One thereby obtains a closed set of equations for single-site and pair probabilities. In addition, hopping terms involving the probabilities of separated pairs of empty sites are factorized as $P[o]^2$. Thus, the pair-approximation yields the equations

$$d/dt\, P[o] = p\cdot P[x] - P[o\,x]^2/P[o] + 4\delta\cdot P[o\,x]\ , \text{ and} \tag{8}$$

$$d/dt\, P[o\,o] = 2p\cdot P[o\,x] - P[o\,x]^2\, P[o\,o]/P[o]^2 - 6\delta\cdot P[o\,o]P[o\,x]/P[o]$$

$$+ 6h(P[o]^2 - P[o\,o]),$$

which can be closed using P[x] = 1-P[o] and P[xo] = P[o]-P[oo].

Below, it is convenient to introduce the conditional probability or concentration, K = P[xo]/P[o], of finding a particle adjacent to a prescribed empty site. Due to spatial correlations, K is distinct from the concentration C = P[x] = 1-P[o]. Then, noting that P[xo] = K(1-C) and that P[o o] = (1-K)(1-C), the pair-approximation then yields the kinetic equations

$$(1\text{-}C)^{-1}\, d/dt\, C = p\cdot C/(1\text{-}C) - K^2 - 4\delta\cdot K, \text{ and}$$
$$(1\text{-}C)^{-1}\, d/dt\, [(1\text{-}K)(1\text{-}C)] = [2p - K(1\text{-}K) - 6\delta(1\text{-}K)]K + 6h(K\text{-}C)\,. \quad (9)$$

The hopping term in the second equation of (9) forces $K \to C$ as $h \to \infty$, thus correctly recovering mean-field behavior corresponding to the absence of spatial correlations.

Our primary interest is in the analysis of steady-state behavior where dC/dt=dK/dt=0. Eliminating C from the steady-state form of (9) yields

$$[2p\text{-}K(1\text{-}K)\text{-}6\delta(1\text{-}K)][p+K^2+4\delta K] + 6h[p\text{-}K(1\text{-}K)\text{-}4\delta(1\text{-}K)] = 0 \text{ or } K = 0. \quad (10)$$

The motivation for selecting K as the natural variable over C is particularly clear for the case h=0, now analyzed in more detail (as for our simulations in Sec.3). Note also that in general one can simply determine p= p(K) as a function of K from (10) by solving a quadratic equation.

For the QCP+SCP with h=0, the steady-state relation (10) reduces to 2p-K(1-K)-6δ(1-K)=0. Thus, analysis of tricritical behavior is no more difficult than for the mean-field treatment corresponding to $h \to \infty$. It is readily shown that when $\delta < \delta_{tc}(\text{pair}) = 1/6$ for h=0, the model displays bistability of an active populated and vacuum state provided that $p_{s-}(\delta) < p < p_{s+}(\delta)$. The upper and lower spinodals predicted from the pair-approximation satisfy

$$p_{s-}(\delta) = 3\delta \text{ and } p_{s+}(\delta) = (1+6\delta)^2/8 = 3\delta + (1\text{-}6\delta)^2/8. \quad (11)$$

For $p<p_{s-}$ ($p>p_{s+}$), only the active (vacuum) state is stable. Bistability disappears at a tricritical point $\delta = \delta_{tc}(pair)=1/6$ for h=0. For $\delta>\delta_{tc}(pair)$ one instead finds a continuous transition at $p=p_{cts}(\delta) =3\delta$ from a unique stable active steady-state exists for $p<p_{cts}(\delta)$ to a unique stable vacuum state for $p>p_{cts}(\delta)$ [27]. A more complete analysis of pair-approximation predictions for steady-state behavior when h=0 is shown in **Fig.8**. This is the analogue of **Fig.2** for $h=\infty$ mean-field behavior where $\delta_{tc}(mf) = ¼$, and of **Fig.4a** for simulated behavior with h=0 where $\delta_{tc}(h=0) \approx 0.034$.

4B. EQUISTABILITY FOR $\delta<\delta_{tc}$

For a comprehensive analysis of pair-approximation behavior and comparison with simulation predictions for h=0 (or any finite h>0), it is necessary to determine equistability values for p in the bistable region when $\delta<\delta_{tc}(pair)$. This requires consideration of spatially non-uniform states, specifically the evolution of planar interfaces separating stable active and vacuum states. To this end, it is necessary to apply the pair-approximation to the spatially-non-uniform version of the hierarchical master equations (1) and (2) which were discussed briefly in Sec.2. This yields a coupled set of discrete RDE's for site dependent particle concentration, $C_{i,j}$, and for related pair probabilities. For a development of such equations in the pair-approximation for the QCP, see Ref.[24] for h=0 and Ref.[31] for h>0. For lower-level site-approximation developments of such equations for other reaction-diffusion models, see Ref.[32-33]. Analysis of interface propagation described by these equations reveals a dependence on orientation, just as seen in simulation studies of the QCP+SCP. Specifically, we find that the equistability value of p depends on interface orientation, corresponding to generic two-phase coexistence.

For the QCP+SCP with h=0, results for the distinct equistability values of $p=p_{eq}$ for horizontal (or vertical) and for diagonal interfaces as predicted from the pair-approximation are shown in **Table IV** for various δ. These values quickly merge with increasing δ, just as do p_e and p_f in the simulation analysis for h=0 (although merging for the latter is even faster; cf. **Table**

I). **Fig. 9** shows pair-approximation prediction for the phase diagram in the p-δ plane for the QCP+SCP model with h=0 including the spinodal lines, $p=p_{s\pm}(\delta)$, and the equistability line, $p=p_{eq}(\delta)$, for $\delta<\delta_{tc}(pair)=1/6$ which merge at $\delta=\delta_{tc}$. The continuation of these lines for $\delta>\delta_{tc}(pair)$ is given by $p=p_{cts}(\delta)=3\delta$ corresponding to the continuous transition. The mean-field analogue of this plot is provided by **Fig.3**, and the simulation analogue is provided by **Fig.4b** (but without spinodal lines).

Finally, for the general QCP+SCP with h≥0, **Fig.10** presents the results of a pair-approximation steady-state analysis based on (9) to determine the tricritical line $\delta_{tc}(pair)$ versus h. The analogue of this plot from simulation studies is provided by **Fig.7**. In both cases, $\delta_{tc}(pair)$ increases monotonically with h reaching the same mean-field value of $\delta_{tc}(mf) = ¼$ for $h=\infty$. However, the pair-approximation is not able to quantitatively predict δ_{tc} for small h.

5. CONCLUSIONS

In summary, we have provided a comprehensive analysis of tricritical behavior in a lattice-gas realization of a hybrid version of Schloegl's first and second models for autocatalysis with particle diffusion on a square lattice. This model also corresponds to a hybrid of the standard Contact Process (SCP) and Quadratic Contact process (QCP). A specific goal was to map out the tricritical line as a function of hop rate showing convergence to the mean-field value in the limit of rapid hopping. In addition, we provided a detailed analysis of tricritical behavior for the case without particle hopping, determining an "epidemic exponent". We note that a previous study considered a modified version of this hybrid model on various lattices but without particle hopping, and obtained various other exponents related to tricritical behavior [15]. Finally, we mention that the general behavior analyzed in this work should apply to a variety of non-equilibrium reaction-diffusion models combining kinetics producing first- and second-order transitions. In Appendix A, we describe another such model and provide an approximate analytic treatment of tricriticality. Corresponding simulation results are presented in Appendix B.

ACKNOWLEDGEMENTS

This work was supported by the Division of Chemical Sciences of the U.S. Department of Energy (USDOE) - Basic Energy Sciences through the Ames Laboratory Chemical Physics FWP. Ames Laboratory is operated for the USDOE by Iowa State University under Contract No. DE-AC02-07CH11358. DU was also supported by NSF REU Grant CHE-0453444.

APPENDIX A: TRICRITICALITY IN A QCP+MCP MODEL: ANALYTIC THEORY

The hybrid QCP+SCP model above includes particle creation via two distinct "parallel" mechanisms at empty sites with k≥1 adjacent diagonal occupied pairs. See **Fig.1**. It is thus natural to modify this model replacing the SCP mechanism with one that is not operative for those configurations where the QCP is operative. We choose this Modified Contact Process or MCP such that particle creation occurs with rate δ, say, only at empty sites with exactly one filled neighboring site. Thus, we consider a hybrid QCP+MCP model with: (i) particle annihilation ate rate p: (ii) particle hopping to adjacent empty sites at rate h (per direction); and (iii) particle creation via both the QCP and MCP mechanisms [34].

For spatially uniform states, the exact form of the hierarchical master equation yields

$$\mathrm{d/dt}\ P[o] = p\cdot P[x] - P\begin{bmatrix} x & \\ o & x \end{bmatrix} - 4\delta\cdot P\begin{bmatrix} & o & \\ o & o & x \\ & o & \end{bmatrix} \qquad \text{(A1)}$$

$$\mathrm{d/dt}\ P[o\quad o] = 2p\cdot P[o\quad x] - P\begin{bmatrix} & x & \\ o & o & x \end{bmatrix} - 2\delta\cdot P\begin{bmatrix} & o & \\ o & o & x \\ & o & \end{bmatrix} - 4\delta\cdot P\begin{bmatrix} & x & \\ o & o & o \\ & o & \end{bmatrix}$$

$$+ 2h\cdot\left(P[o\quad -\quad o] + 2\cdot P\begin{bmatrix} & o \\ o & - \end{bmatrix} - 3\cdot P[o\quad o] \right) \qquad \text{(A2)}$$

and where P's in the two MCP loss terms in (A2) are equivalent so these terms can be combined.

A mean-field analysis of the QCP+MCP starts with the generalized version of (A1) for spatially non-uniform states. For a coarse-grained particle concentration, C=C(r=(i,j)a), where 'a' denotes the lattice constant, this analysis yields the reaction-diffusion equation (RDE)

$$\partial C/\partial t = R^*(C) + D\,\nabla^2 C \text{ with } R^*(C) = -p\cdot C + C^2(1-C) + 4\delta\cdot C(1-C)^4, \qquad (A3)$$

and where $D=a^2 h$. Any stable uniform active steady state satisfies $p=C(1-C)+4\delta(1-C)^4$ and the vacuum steady state has C=0. **Fig.11** illustrates the steady-state dependence of C on p for various δ selected to show several distinct steady-state bifurcations (see also **Fig.12**):

(i) For small δ≥0, a high-C stable active state exists for $0 \le p \le p_{s+}(\delta)$, and a stable vacuum state exists for $p \ge p_{s1-}(\delta)$, so the model exhibits bistability in the regime $p_{s1-}(\delta) \le p \le p_{s+}(\delta)$. This is analogous to behavior in the QCP+SCP. Here, one has $p_{s1-}(\delta) = 4\delta$ (just as in the QCP+SCP), and $p_{s+}(\delta) = ¼ + ¼\,\delta + O(\delta^2)$ which increases smoothly with δ. See **Fig.11(a)**.

(ii) For $\delta > \delta_{cts} = 1/16 = 0.0625$, a stable low-C active state develops which coexists with the above stable high-C active state. This low-C state exists for $p_{s2-}(\delta) \le p \le p_{cts}(\delta)$, where $p_{s2-}(\delta) = ¼ + 4(\delta - 1/16) - 256(\delta - 1/16)^2 + \ldots = 4\delta - 256(\delta - 1/16)^2 + \ldots$ for δ≥1/16. Also, $p_{cts}(\delta) = 4\delta$ corresponds to a continuous transition from the stable low-C active state to the stable vacuum state. Thus, bistability exists in the regime $p_{s2-}(\delta) \le p \le p_{s+}(\delta)$. See **Fig.11(b) and (c).**

(iii) As δ increases further above δ_{cts}, $p_{cts}(\delta)$ increases faster than $p_{s+}(\delta)$, so soon both $p_{s2-}(\delta)$ and $p_{s+}(\delta)$ are below $p_c(\delta)$.

(iv) As δ reaches a critical point $\delta_{cp} = 2/27 \approx 0.0741$, $p_{s2-}(\delta)$ and $p_{s+}(\delta)$ merge and bistability disappears. At this critical point, we find that $C_{cp} = ¼$ and $p_{cp} = 9/32 \approx 0.2813$. Also when $\delta = \delta_{cp}$, the continuous transition to the vacuum state persists, but occurs at a slightly higher p-value of $p_{cts} = 4\delta_{cp} = 8/27 \approx 0.2963$. See **Fig.11(d).**

For $\delta<\delta_{cp}$, one can determine $p=p_{eq}(\delta)$ corresponding to equistability between the high-C active and a low-C stable state, where $p_{s-}(\delta) \le p_{eq}(\delta) \le p_{s+}(\delta)$ [35]. $p_{eq}(\delta)$ follows from analysis of

the effective potential U*(C) defined by R*(C) = -dU*/dC, analogous to Sec.2. One finds that $p_{cts}(\delta) = 4\delta$ increases more quickly that $p_{eq}(\delta)$, and consequently $p_{cts}(\delta)$ and $p_{eq}(\delta)$ will coincide at $\delta = \delta_{eq} \approx 0.068$ (between δ_{cts} and δ_{cp}). See **Fig.12**.

Based on the above mean-field analysis, we describe behavior in the QCP+MCP lattice-gas model with large h for various regimes of δ: **(a)** For $0 \le \delta < \delta_{eq}$, one expects a discontinuous transition from a high-C active state to a vacuum state when p increases above $p_{eq}(\delta)$. **(b)** For $\delta_{eq} < \delta < \delta_{cp}$, one expects the discontinuous transition to persist, but instead to occur between the high-C active state and a low-C active state when p increases above $p_{eq}(\delta)$. This low-C active state then undergoes a continuous transition to the vacuum state as p increases to $p_{cts}(\delta)$ which is above $p_{eq}(\delta)$. **(c)** As δ increases to δ_{cp}, the discontinuous transition disappears at a critical point. Critical behavior in Schloegl-type models has been analyzed previously and determined to be in the Ising universality class [36]. **(d)** For $\delta \ge \delta_{cp}$, the continuous transition from an active state to the vacuum state persists.

The above picture of behavior in the QCP+MCP lattice-gas model for various δ likely does not apply for small h. The pair-approximation to the exact master equations described above can be applied in an attempt to more reliably describe behavior for small and finite $h \ge 0$. Here, we consider exclusively the case h=0. We introduce the natural variable K = P[x o]/P[o] as in Sec.4. Then, the pair-approximation produces the steady-state condition $p = \frac{1}{2} K(1-K) + 6\delta(1-K)^3$ or K=0. Behavior is qualitatively distinct from that in mean-field treatment. Specifically, the pair approximation for h=0 predicts a transition directly from bistability to a continuous transition at a tricritical point $\delta_{cp} = 1/18$. Thus, one anticipates that the discontinuous transition for small δ in the QCP+MCP lattice-gas model for h=0 converts directly to a continuous transition at a tricritical point for increasing δ (in contrast to the MF picture). However, in contrast to the general situation for tricitical points, the curvature $d^2C/dp^2|_{tc} = 0$ in the pair-approximation vanishes at the tricritical point (just like at a critical point). Also when $\delta \ge \delta_{tc}$, the continuous transition to the vacuum state occurs at $p_{cts}(\delta) = 3\delta$. See **Fig.13**.

APPENDIX B: TRICRITICALITY IN A QCP+MCP MODEL: SIMULATION RESULTS

We present results from a simulation study for the QCP+MCP with h=0 (with more limited statistics than for the QCP+SCP). **Fig.14** show the results of CC simulations to determine the variation of p with C, but plotted to show C(p) versus p, for a range of δ around what appears to be a tricritical point, $\delta=\delta_{tc}$. From this data, we extract $p_{tr}(\delta) = \lim_{C\to 0} p(C)$, which corresponds the location of the discontinuous transition for $\delta<\delta_{tc}$ (noting that the two-phase coexistence region will have negligible width except for very small δ), and to the location of the continuous transition $p_{cts}(\delta)$ for $\delta>\delta_{tc}$. We also determine $dp/dC|_{C=0}$ versus δ which is around zero or slightly positive for small δ, but makes a transition to significant negative values as δ increases above $\delta_{tc} \approx 0.026$-$0.028$. We have also performed an epidemic analysis to assess the evolution of a single occupied site embedded in the vacuum state. Specifically, we determine the behavior at the transition point, $p=p_{tr}(\delta)$, of the survival probability, $P_s(t)$, versus t, fitting data to the form $P_s(t) \sim t^{-\zeta}$, as $t\to\infty$. For $\delta_{tc} \approx 0.026$-$0.028$, one obtains $\zeta_{tc} = 1.40$-1.58. It is clear that the effective ζ adopts larger (smaller) values for δ significantly smaller (larger) than δ_{tc}, as for the QCP+SCP. See **Fig.15**. Finally, we remark that our estimate of ζ_{tc} for the QCP+MCP is somewhat above that for the QCP+SCP, a feature perhaps related to the proximity of a tricritical and critical point in the QCP+MCP (as suggested by the pair-approximation treatment).

In summary, simulation studies of the QCP+MCP for h=0 indicate that a discontinuous transition for low δ converts directly to a continuous transition (consistent with the pair-approximation) as δ increases above a tricritical value of $\delta_{tc} \approx 0.026$-$0.028$. For large enough h, mean-field behavior must be realized for which there is indirect conversion from a discontinuous to continuous transition via a region of coexistence of both transitions (with the discontinuous transition disappearing at a critical point). Thus, the tricritical line in the (h,δ)-plane emanating from $(h, \delta) \approx (0, 0.027)$ should propagate for a range of $h\geq 0$ before expanding into a region of finite width (in δ) reflecting coexistence of discontinuous and continuous transitions.

REFERENCES

[1] G. Nicolis and I. Prigogine, *Self-Organization in Non-Equilibrium Systems* (Wiley, New York, 1977).

[2] A.S. Mikhailov, *Foundations of Synergetics I* (Springer, Berlin, 1990).

[3] H. Malchow and L. Schimanski-Geier, *Noise and Diffusion in Bistable Nonequilibrium Systems* (Teubner, Berlin, 1985).

[4] J.W. Evans, D.-J. Liu, and M. Tammaro, Chaos **12**, 131 (2002).

[5] J. Marro and R. Dickman, *Nonequilibrium Phase Transitions in Lattice Models* (Cambridge UP, Cambridge, 1999).

[6] H. Hinrichsen, Adv. Phys. **49**, 815 (2000).

[7] G. Odor, Rev. Mod. Phys. **76**, 663 (2004).

[8] R.M. Ziff, E. Gulari, and Y. Barshad, Phys. Rev. Lett. **56**, 2553 (1986).

[9] J.W. Evans and M.S. Miesch, Phys. Rev. Lett. **66**, 833 (1991).

[10] J.W. Evans and T.R. Ray, Phys. Rev. E, **50**, 4302 (1994).

[11] R. H. Goodman, D. S. Graff, L. M. Sander, P. Leroux-Hugon, and E. Clément Phys. Rev. E **52**, 5904 (1995).

[12] E. Loscar and E.V. Albano, Rep. Prog. Phys. **66**, 1343 (2003).

[13] E. Machado, G.M. Buendia, and P.A. Rikvold, Phys. Rev. E **71**, 031603 (2005).

[14] D.-J. Liu, X. Guo, and J.W. Evans, Phys. Rev. Lett. **98**, 050601 (2007).

[15] S. Luebeck, J. Stat. Phys. 123, 193 (2006).

[16] F. Schloegl, Z. Phys. **253**, 147 (1972).

[17] P. Grassberger, Z. Phys. B Cond. Matt. **47**, 365 (1982).

[18] J.P. Boon, D. Dab, R. Kapral, and A. Lawniczak, Rep. Mod. Phys. **273**, 55 (1996).

[19] S. Prakash and G. Nicolis, J. Stat. Phys. **86**, 1289 (1997).

[20] R. Durrett, SIAM Rev. **41**, 677 (1999).

[21] X. Guo, D.-J. Liu, and J.W. Evans, Phys. Rev. E, **75**, 061129 (2007).

[22] X. Guo, D.-J. Liu, and J.W. Evans, J. Chem. Phys. **130**, 074106 (2009).

[23] J.W. Evans, Rev. Mod. Phys. **65**, 1281 (1993).

[24] X. Guo, J.W. Evans, and D.-J. Liu, Physica A **387**, 177 (2008).

[25] J.W. Evans and D.K. Hoffman, Phys. Rev. B **30**, 2704 (1984).

[26] R. Kutner, Phys. Lett. **81A**, 239 (1981).

[27] In either regime, the active steady-state coverage satisfies $2C_{eq} =(1-4d)+[(1-4d)^2-4(p-4d)]^{1/2}$.

[28] The decrease of Δp_{eq} with δ is very similar to that for a related model where the SCP mechanism is replaced by spontaneous creation at empty sites at rate δ. See D.-J. Liu, J. Stat. Phys. **135**, 77 (2009). Note that for a high-concentration active state, there should not be much difference between the SCP mechanism and spontaneous creation.

[29] R.M. Ziff and B.J. Brosilow, Phys. Rev. A **46**, 4630 (1992).

[30] R. Dickman, Phys. Rev. A **34**, 4246 (1986).

[31] X. Guo, Y. De Decker, and J.W. Evans, Phys. Rev. E, **82**, 021121 (2010).

[32] P. Fischer and U.M. Titulaer, Surf. Sci. **221**, 409 (1989).

[33] Y. De Decker, G.A. Tsekouras, A. Provata, Th. Erneux, and G. Nicolis, Phys. Rev. E **69**, 036203 (2004).

[34] For the QCP+MCP, the particle creation rate at an empty site completely surrounded by four filled sites equals 1, so that $C_{eq}(p) = 1-p + O(p^2)$ independent of h (contrasting the QCP+SCP).

[35] $p_{s-}(\delta)$ corresponds to $p_{s1-}(\delta)$ and $p_{s2-}(\delta)$ for $\delta<\delta_{cts}$ and $\delta>\delta_{cts}$, respectively.

[36] D.-J. Liu, J. Stat. Phys. **135**, 77 (2009).

TABLE I: CC-simulation values of p_e and p_f versus δ for the QCP+SCP with h=0.

δ	p_f	p_e	$\Delta p_{eq} = p_e - p_f$
0	0.0869	0.09443	0.0075
0.0001	0.0901	0.09456	0.0045
0.0002	0.0910	0.09503	0.0040
0.0005	0.0929	0.09549	0.0026
0.001	0.0947	0.09622	0.0015
0.002	0.0974	0.09798	0.0006

TABLE II: Location of the transition $p=p_{tr}(\delta)$ for the QCP+SCP with h=0.

δ	p_{tr}
0.01	0.11554
0.02	0.13622
0.03	0.15669
0.04	0.17787
0.05	0.19941
0.06	0.22203
0.07	0.24490

TABLE III: Values of parameters ζ_1 and ζ_2 versus δ for the QCP+SCP with h=0.

δ	ζ_1	ζ_2
0.030	1.474	-0.070
0.032	1.506	-0.073
0.034	1.202	0.010
0.036	1.041	0.024
0.038	0.927	0.043
0.040	0.779	0.097

TABLE IV: Pair-approximation prediction of equistability points in the QCP+SCP with h=0.

δ	p_{eq}(horiz/vert = h/v)	p_{eq}(diag)	$\Delta p_{eq} = p_{eq}$(diag)-p_{eq}(h/v)
0.0	0.1060	0.1083	0.0023
0.01	0.12530	0.12607	0.00077
0.02	0.14416	0.14447	0.00031

0.03	0.16342	0.16356	0.00014
0.04	0.18329	0.18336	0.00007
0.10	0.31772	0.31772	<0.00001
1/6	1/2	1/2	0

FIGURE CAPTIONS

Figure 1. Schematic of particle annihilation, autocatalytic creation, and hopping processes in our generalized Schloegl model (QCP+SCP) on a square lattice. Here particles are denoted by filled circles (•) and empty sites by open circles (o). Rates for the various processes are also indicated, and the bar through the arrow indicates that the process is inactive.

Figure 2: Mean-field steady-state behavior for particle concentration, C, versus p in the QCP+SCP. For $\delta < \delta_{tc} = ¼$ below the tricritical point (tc), we show upper (s+) and lower (s-) spinodals bordering the region of bistability. For $\delta>\delta_{tc}$, we show the location of the continuous transition (cts) to the vacuum state.

Figure 3: Phase diagram in the p-δ plane for the mean-field QCP+SCP including the spinodal lines, $p=p_{s\pm}(\delta)$, and the equistability line, $p=p_{eq}(\delta)$, for $\delta<\delta_{tc}$ below the tricritical point (tc) which merge at $\delta=\delta_{tc}=1/4$. The continuation of these lines, $p=p_{cts}(\delta)=4\delta$, for $\delta>\delta_{tc}$ corresponds to the continuous transition.

Figure 4: Simulation analysis of the QCP+SCP for h=0: (a) Results of CC simulations for p versus C used to determine the location of the transition, $p=p_{tr}(\delta)$ versus δ from $C(p_{tr}(\delta))=0$; (b) Plot of results for $p_{tr}(\delta)$ versus δ obtained from (a), also showing the tricritical point (tc). The inset shows p_e (lower curve) and p_f (upper curve) versus δ for a range of very small δ where they are significantly different.

Figure 5: Epidemic analysis for the QCP+SCP with h=0. Survival probability, $P_s(t)$, versus time, t, for a single occupied site embedded in the vacuum state for various δ choosing $p=p_{tr}(\delta)$ with values given in Table II. The inset shows behavior for a broad range of δ varying between 0.01 and 0.07 in increments of 0.01. The main plot shows high-quality data in the vicinity of the tricritical point used to estimate $\delta_{tc} \approx 0.0338\pm0.0010$ and $\zeta_{tc} \approx 1.23\pm0.10$.

Figure 6: CC simulation results for the QCP+SCP with h=0.5 showing p versus C (or equivalently C versus p) for various δ. This data is used to estimate the tricritical point, $\delta_{tc}(h=0.5) \approx 0.070$.

Figure 7: Simulation results for the tricritical line, $\delta_{tc}(h)$, versus h for the general QCP+SCP with $h\geq0$. This line separates regions of discontinuous (below) and continuous (above) transitions.

Figure 8: Pair-approximation predictions for steady-state behavior for particle concentration, C, versus p in the QCP+SCP with h=0. For $\delta<\delta_{tc} = 1/6$ below the tricritical point (tc), we show upper (s+) and lower (s-) spinodals bordering the region of bistability. For $\delta>\delta_{tc}$, we show the location of the continuous transition (cts) to the vacuum state.

Figure 9: Pair-approximation predictions for the phase diagram in the p-δ plane for the mean-field QCP+SCP with h=0. Included are the spinodal lines, $p=p_{s\pm}(\delta)$, and the equistability line, $p=p_{eq}(\delta)$, for $\delta<\delta_{tc}$ which merge at the tricritical point (tc) $\delta=\delta_{tc}=1/6$. The continuation of these lines for $\delta>\delta_{tc}$ is given by $p=p_{cts}(\delta)=3\delta$ corresponding to the continuous transition. The inset shows distinct values for p_{eq} for horizontal or vertical interfaces (lower curve) and for diagonal interfaces (upper curve) versus δ for a range of very small δ where they are significantly different.

Figure 10: Pair-approximation predictions for the tricritical line, $\delta_{tc}(h)$, versus h for the general QCP+SCP with $h\geq 0$. This line separates regions of bistability (below) and monostability (above).

Figure 11: Mean-field variation of steady-state C(p) with p in the QCP+MCP: (a) $\delta<\delta_{cts}$; (b) $\delta_{cts} < \delta < \delta_{eq}$; (c) $\delta_{eq} < \delta < \delta_{cp}$; (d) $\delta = \delta_{cp}$. The notation s+ and s- indicates upper and lower spinodals, respectively; cp indicates the critical point, and cts the continuous transition.

Figure 12: Schematic of the mean-field phase-diagram in the p-δ plane for the QCP+MCP. The diagram is distorted from quantitative behavior in order to highlight key features.

Figure 13: Pair-approximation prediction for variation of steady-state C(p) with p in the QCP+MCP with h=0: (a) $\delta=0$; (b) $0 < \delta < \delta_{tc}$; (c) $\delta = \delta_{tc} = 1/18$; (d) $\delta > \delta_{tc}$. The notation s+ and s- indicates upper and lower spinodals, respectively; tc indicates the tricritical point, and cts the continuous transition.

Figure 14: CC simulation results for steady-state behavior in the QCP+MCP with h=0 for various δ. From this data, we estimate that $\delta_{ct} \approx 0.026\text{-}0.028$.

Figure 15: Epidemic analysis for the QCP+MCP with h=0. Survival probability, $P_s(t)$, versus time, t, for a single occupied site embedded in a vacuum state for $0.021<\delta<0.035$, and choosing $p = p_{tr}(\delta)$. For $\delta_{tc} \approx 0.026\text{-}0.028$, one obtains $\zeta_{tc} = 1.40\text{-}1.58$.

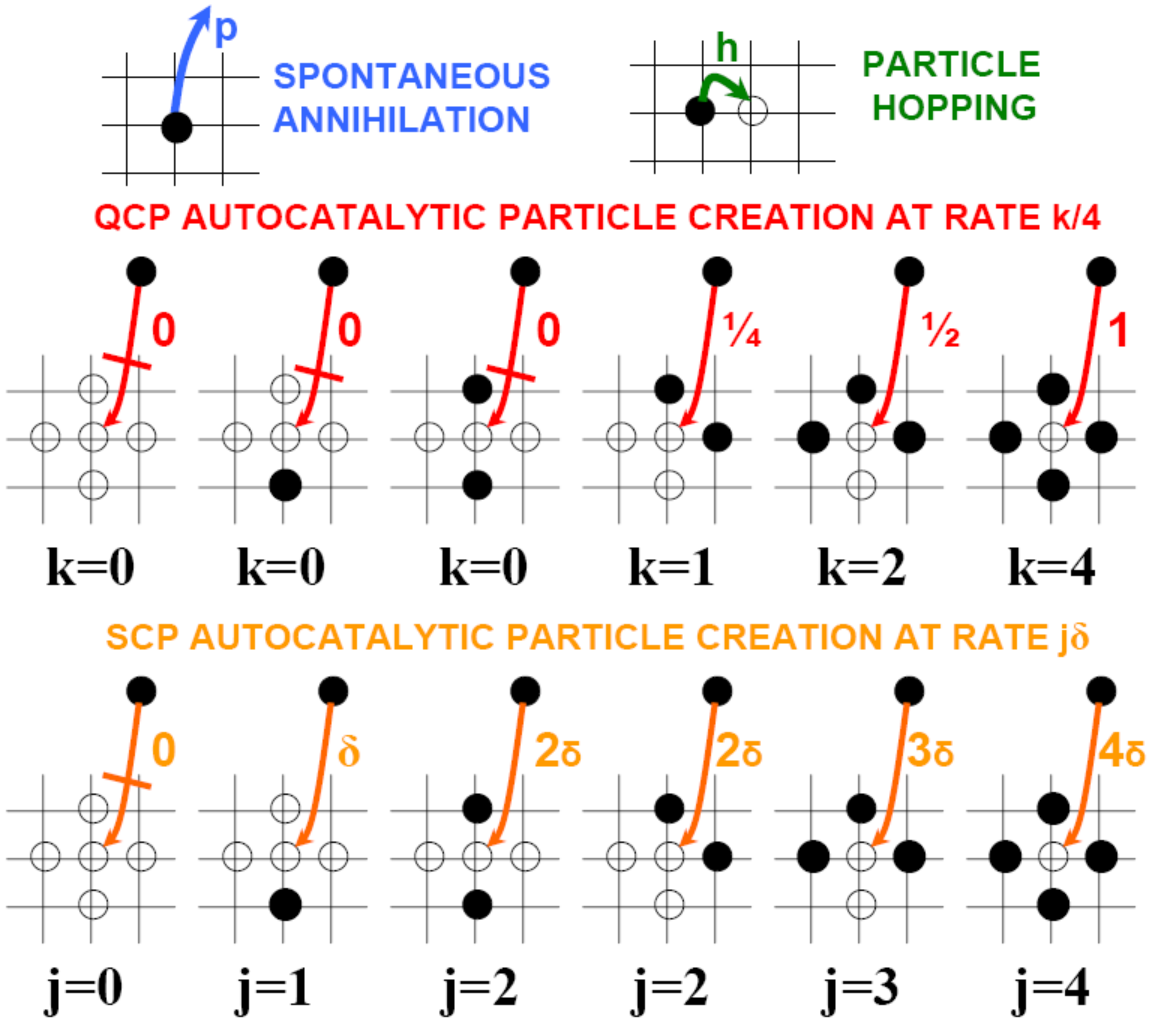

Figure 1. Schematic of particle annihilation, autocatalytic creation, and hopping processes in our generalized Schloegl model (QCP+SCP) on a square lattice. Here particles are denoted by filled circles (•) and empty sites by open circles (o). Rates for the various processes are also indicated, and the bar through the arrow indicates that the process is inactive.

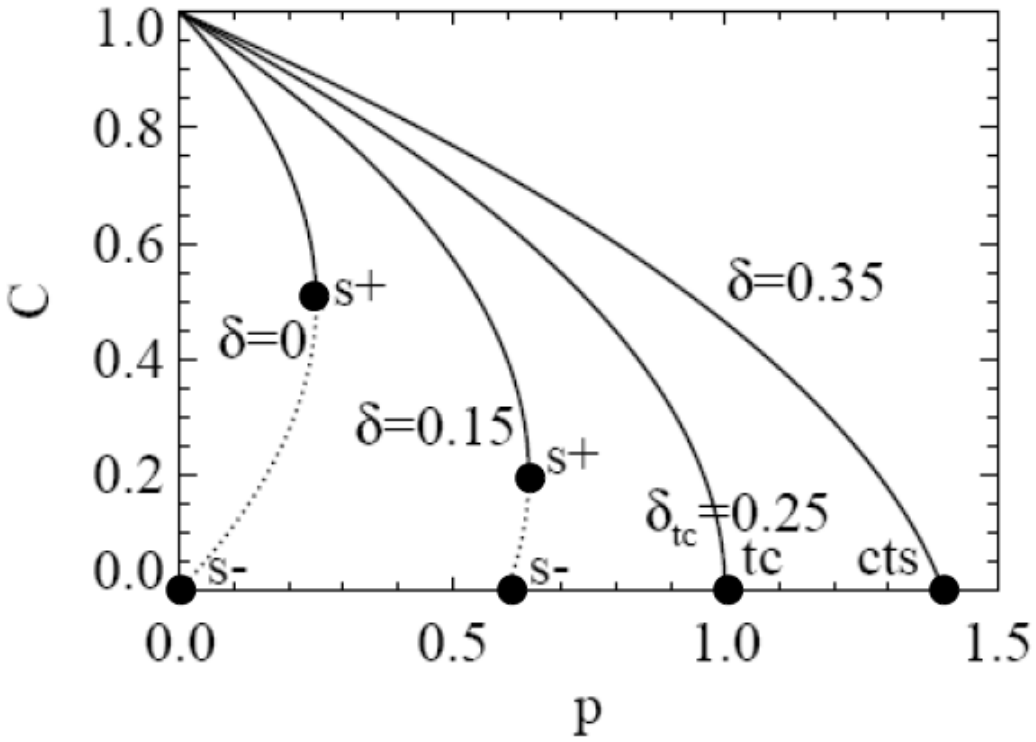

Figure 2: Mean-field steady-state behavior for particle concentration, C, versus p in the QCP+SCP. For $\delta<\delta_{tc} = ¼$ below the tricritical point (tc), we show upper (s+) and lower (s-) spinodals bordering the region of bistability. For $\delta>\delta_{tc}$, we show the location of the continuous transition (cts) to the vacuum state.

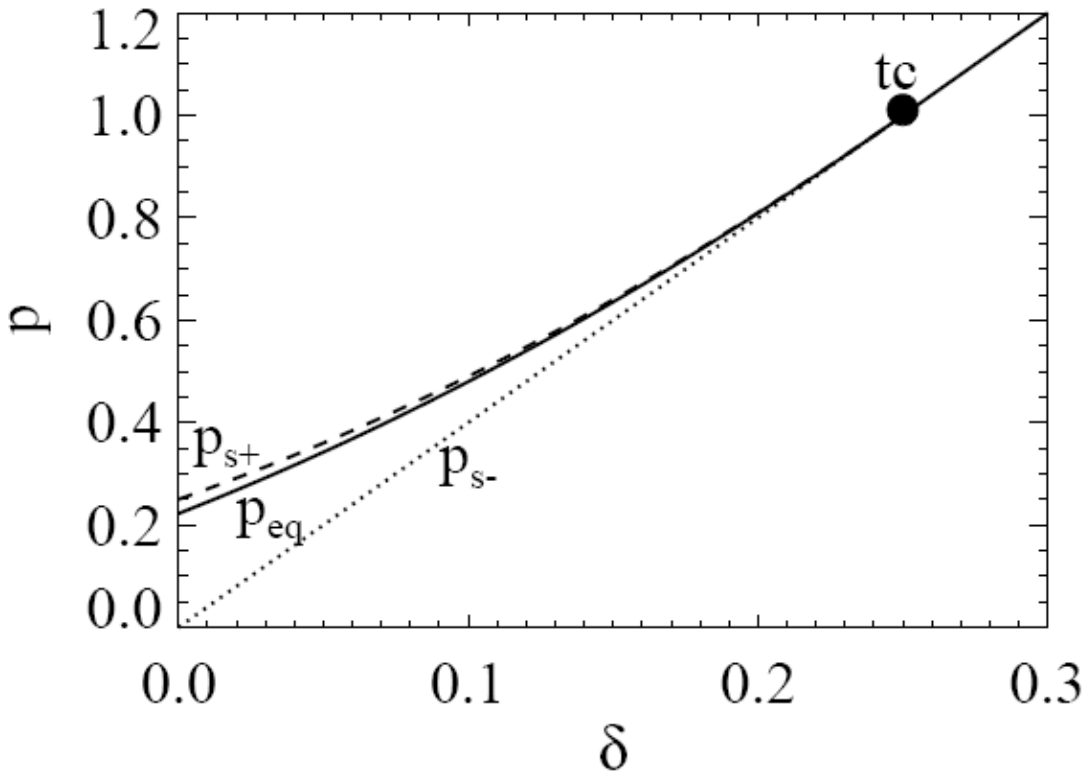

Figure 3: Phase diagram in the p-δ plane for the mean-field QCP+SCP including the spinodal lines, $p=p_{s\pm}(\delta)$, and the equistability line, $p=p_{eq}(\delta)$, for $\delta<\delta_{tc}$ below the tricritical point (tc) which merge at $\delta=\delta_{tc}=1/4$. The continuation of these lines, $p=p_c(\delta)=4\delta$, for $\delta>\delta_{tc}$ corresponds to the continuous transition.

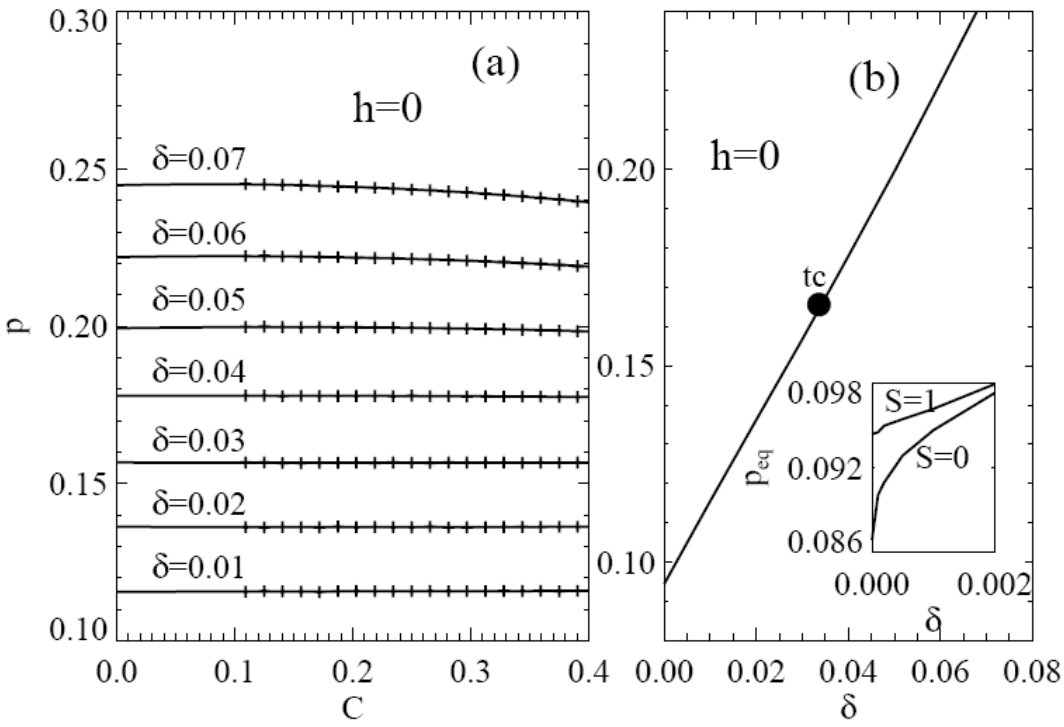

Figure 4: Simulation analysis of the QCP+SCP for h=0: (a) Results of CC simulations for p versus C used to determine the location of the transition, $p=p_{tr}(\delta)$, versus δ from $C(p_{tr}(\delta))=0$; (b) Plot of results for $p_{tr}(\delta)$ versus δ obtained from (a), also showing the tricritical point (tc). The inset shows p_e (lower curve) and p_f (upper curve) versus δ for a range of very small δ where they are significantly different.

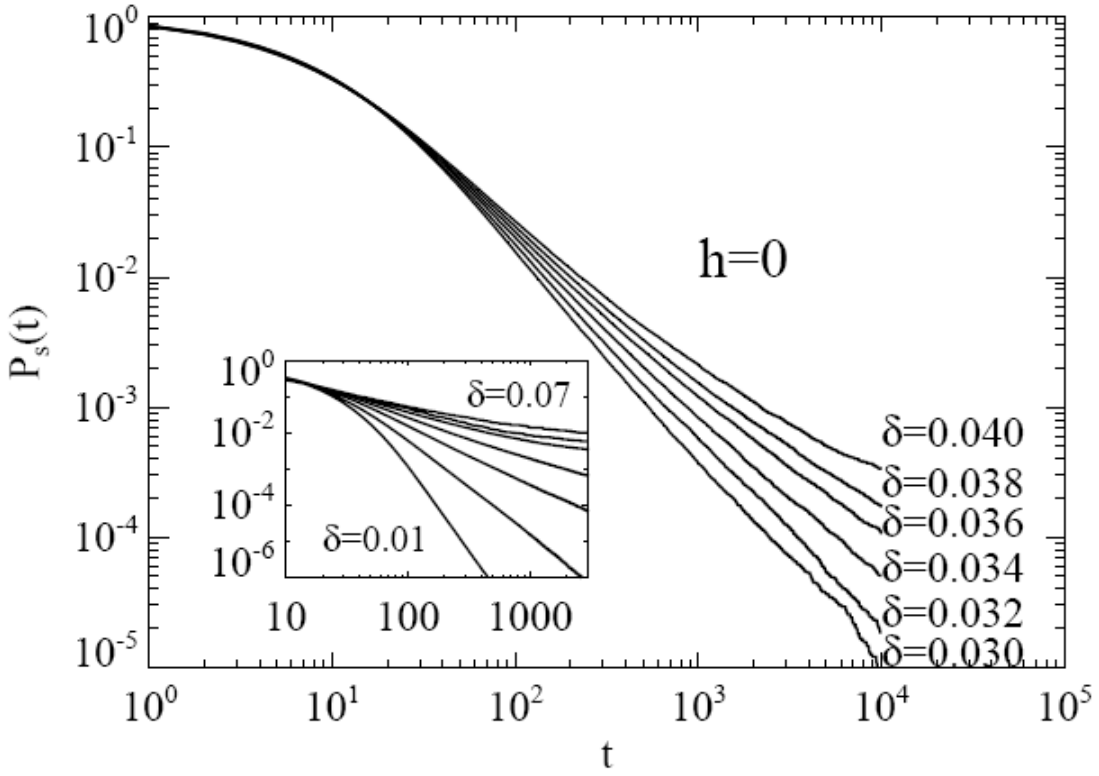

Figure 5: Epidemic analysis for the QCP+SCP with h=0. Survival probability, $P_s(t)$, versus time, t, for a single occupied site embedded in the vacuum state for various δ choosing $p=p_{tr}(\delta)$ with values given in Table II. The inset shows behavior for a broad range of δ varying between 0.01 and 0.07 in increments of 0.01. The main plot shows high-quality data in the vicinity of the tricritical point used to estimate $\delta_{tc} \approx 0.0338 \pm 0.0010$ and $\zeta_{tc} \approx 1.23 \pm 0.10$.

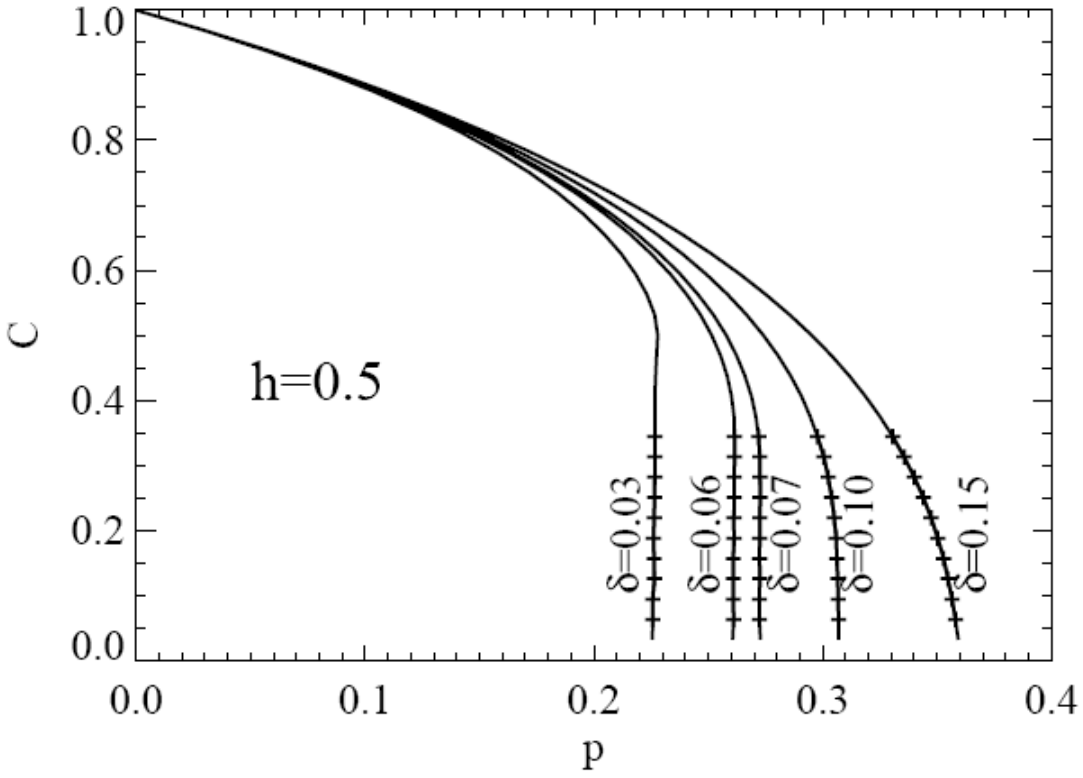

Figure 6: CC simulation results for the QCP+SCP with h=0.5 showing p versus C (or equivalently C versus p) for various δ. This data is used to estimate $\delta_{tc}(h=0.5) \approx 0.070$.

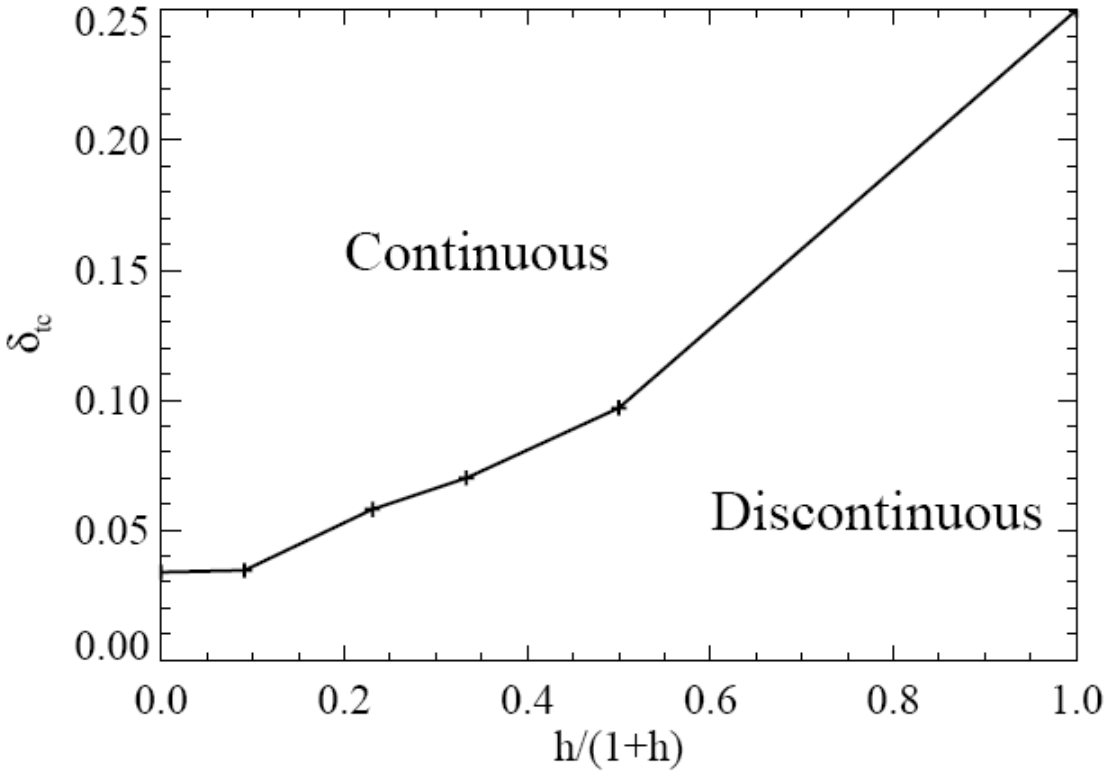

Figure 7: Simulation results for the tricritical line, $\delta_{tc}(h)$, versus h for the general QCP+SCP with $h \geq 0$. This line separates regions of discontinuous (below) and continuous (above) transitions.

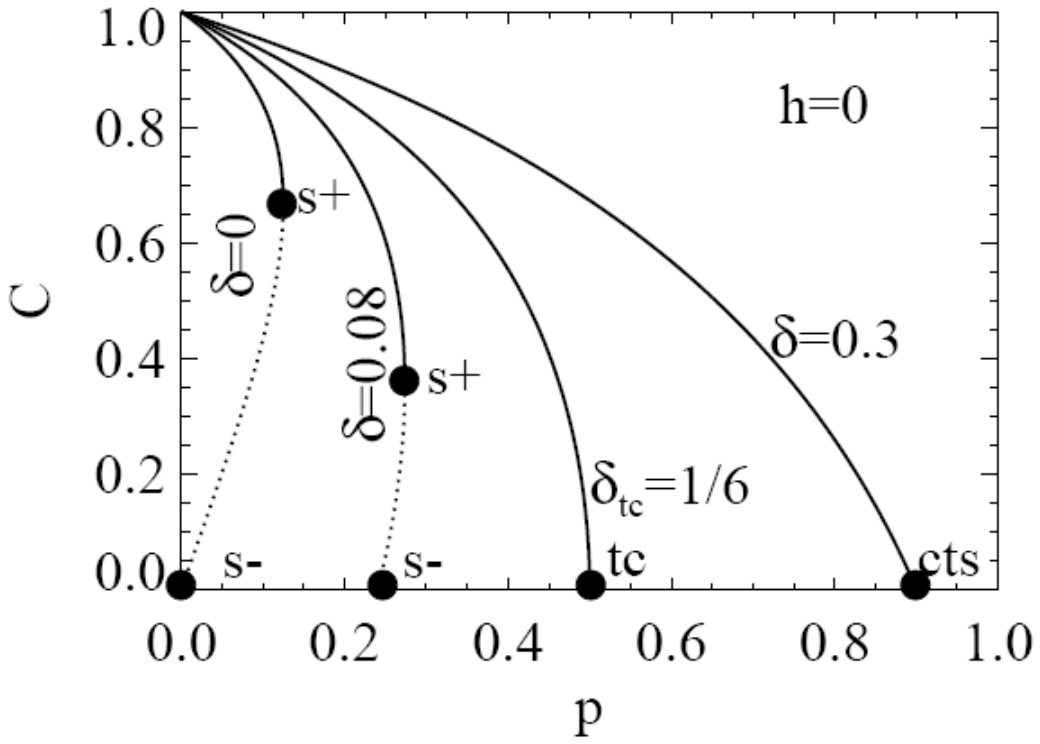

Figure 8: Pair-approximation predictions for steady-state behavior for particle concentration, C, versus p in the QCP+SCP with h=0. For $\delta<\delta_{tc} = 1/6$ below the tricritical point (tc), we show upper (s+) and lower (s-) spinodals bordering the region of bistability. For $\delta>\delta_{tc}$, we show the location of the continuous transition (cts) to the vacuum state.

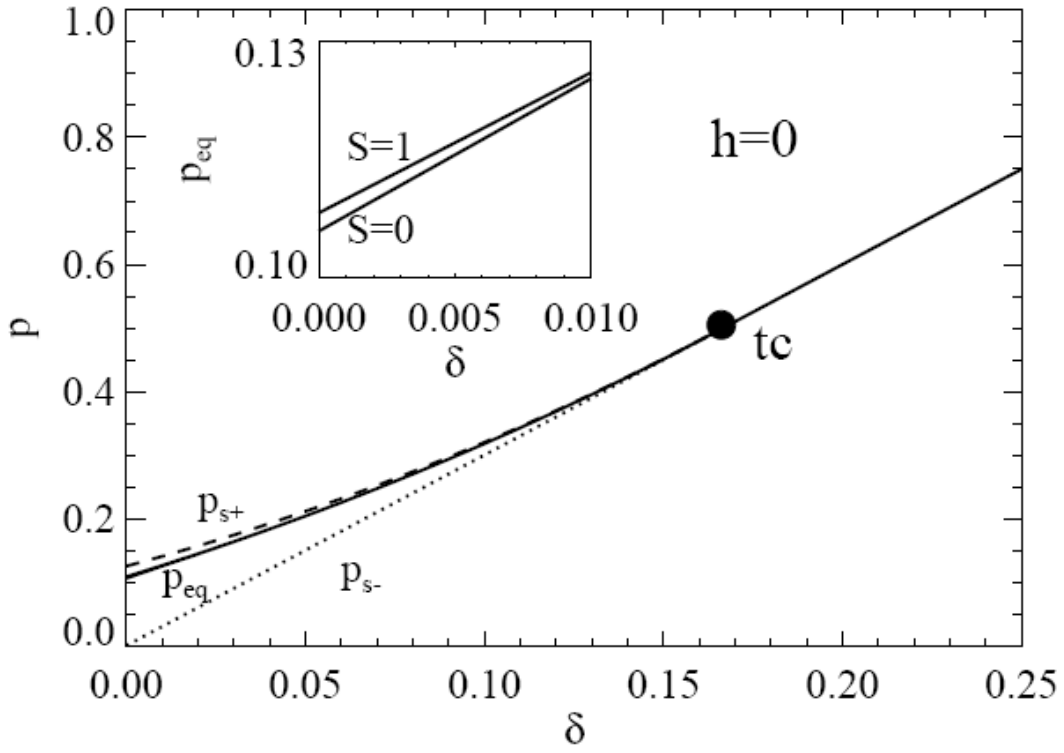

Figure 9: Pair-approximation predictions for the phase diagram in the p-δ plane for the mean-field QCP+SCP with h=0. Included are the spinodal lines, $p=p_{s\pm}(\delta)$, and the equistability line, NOTICE: this is the author's version of a work that was accepted for publication in Physica A: Statistical Mechanics and its Applications. Changes resulting from the publishing process, such as peer review, editing, ocorrections, structural formatting, and other quality control mechanisms may not be reflected in this document. Changes may have been made to this work since it was submitted for publication. A definitive version was subsequently published in Physica A: Statistical Mechanics and its Applications, vol.391, issue 3, (2012), doi: 10.1016/j.physa.2011.08.049.

$p=p_{eq}(\delta)$, for $\delta<\delta_{tc}$ which merge at the tricritical point (tc) $\delta=\delta_{tc}=1/6$. The continuation of these lines for $\delta>\delta_{tc}$ is given by $p=p_c(\delta)=3\delta$ corresponding to the continuous transition. The inset shows distinct values for p_{eq} for horizontal or vertical interfaces (lower curve) and for diagonal interfaces (upper curve) versus δ for a range of very small δ where they are significantly different.

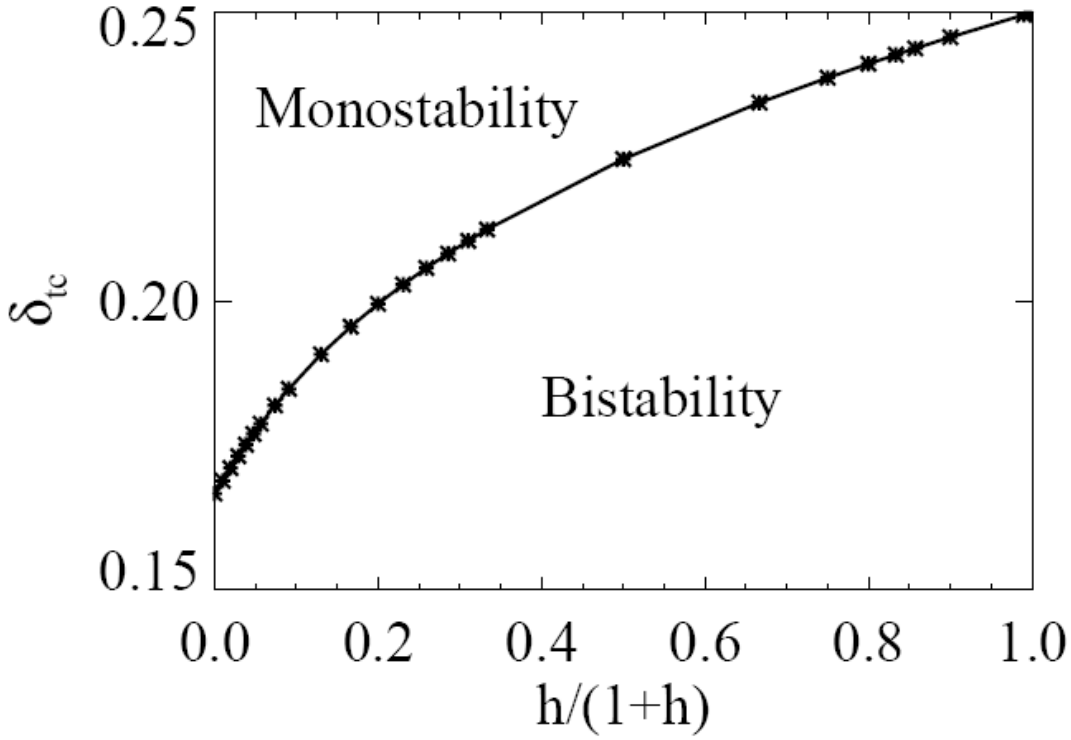

Figure 10: Pair-approximation predictions for the tricritical line, $\delta_{tc}(h)$, versus h for the general QCP+SCP with $h \geq 0$. This line separates regions of bistability (below) and monostability (above).

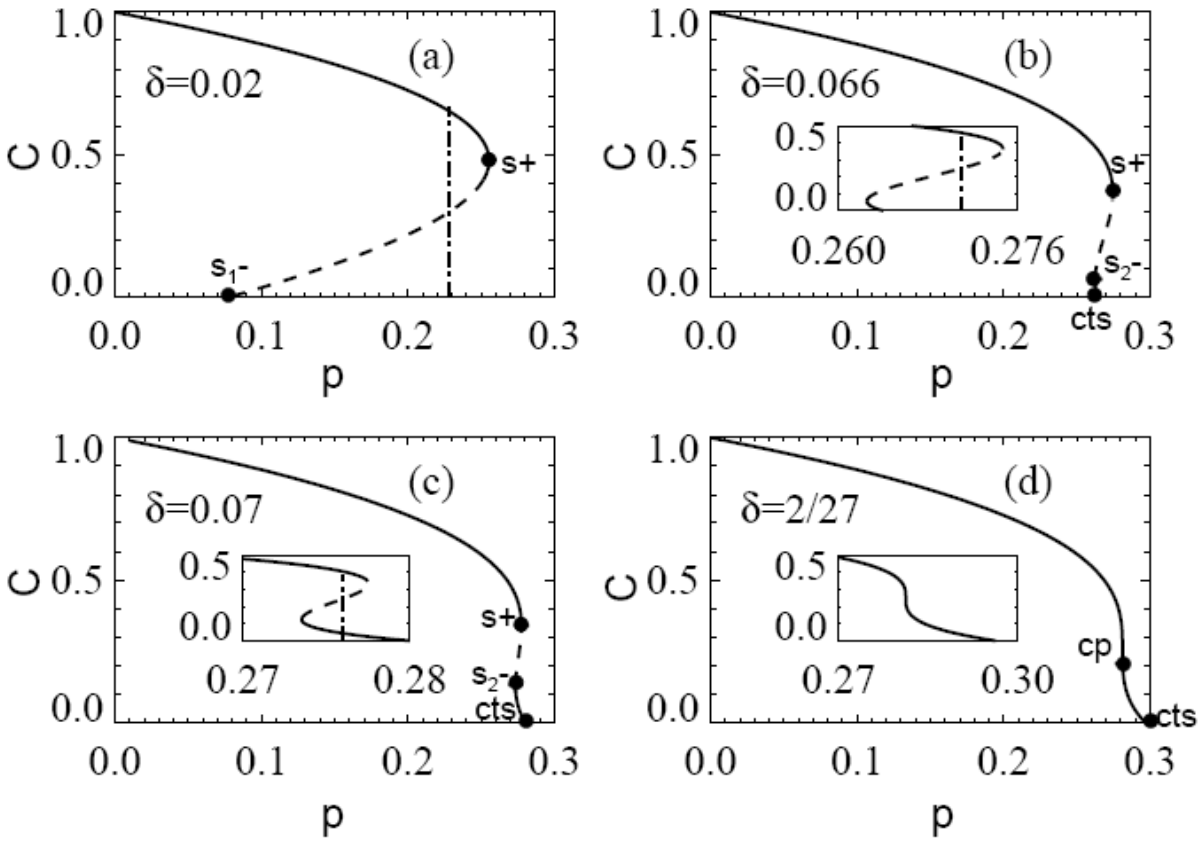

Figure 11: Mean-field variation of steady-state C(p) with p in the QCP+MCP: (a) $\delta<\delta_{cts}$; (b) $\delta_{cts} < \delta < \delta_{eq}$; (c) $\delta_{eq} < \delta < \delta_{cp}$; (d) $\delta = \delta_{cp}$. The notation s+ and s- indicate upper and lower spinodals, respectively; cp indicates the critical point, and cts the continuous transition.

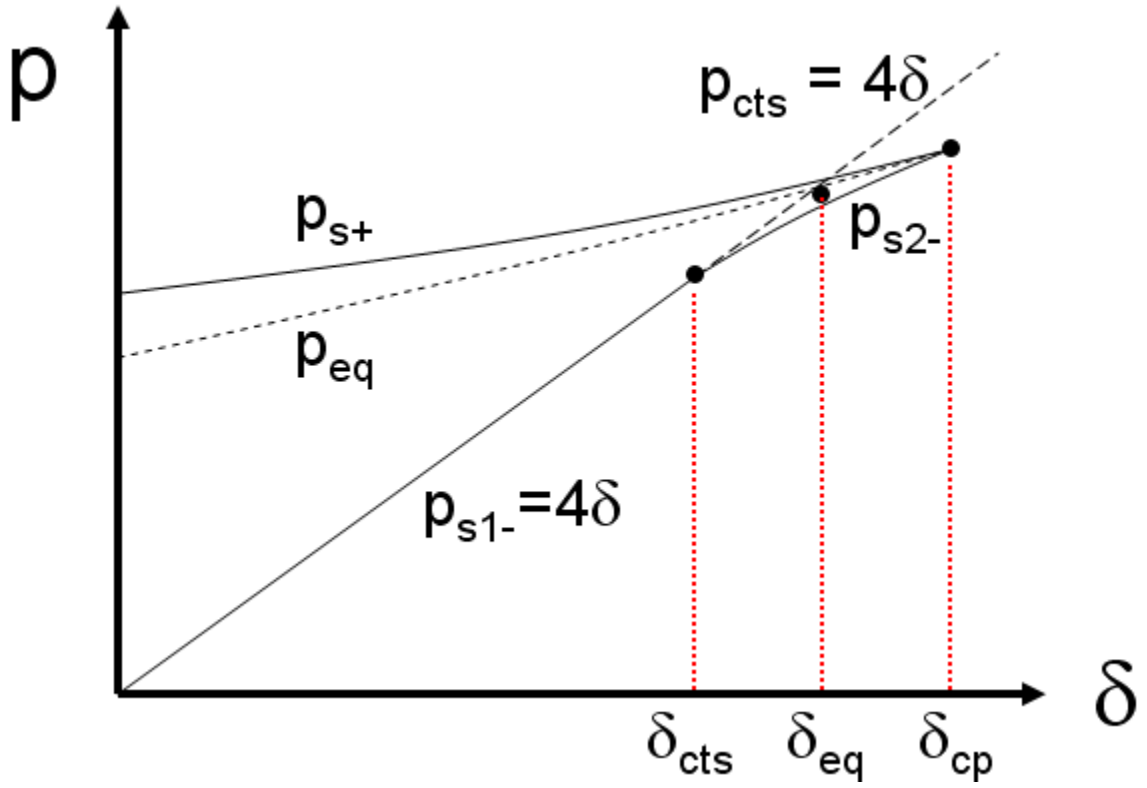

Figure 12: Schematic of the mean-field phase-diagram in the p-δ plane for the QCP+MCP. The diagram is distorted from quantitative behavior in order to highlight key features.

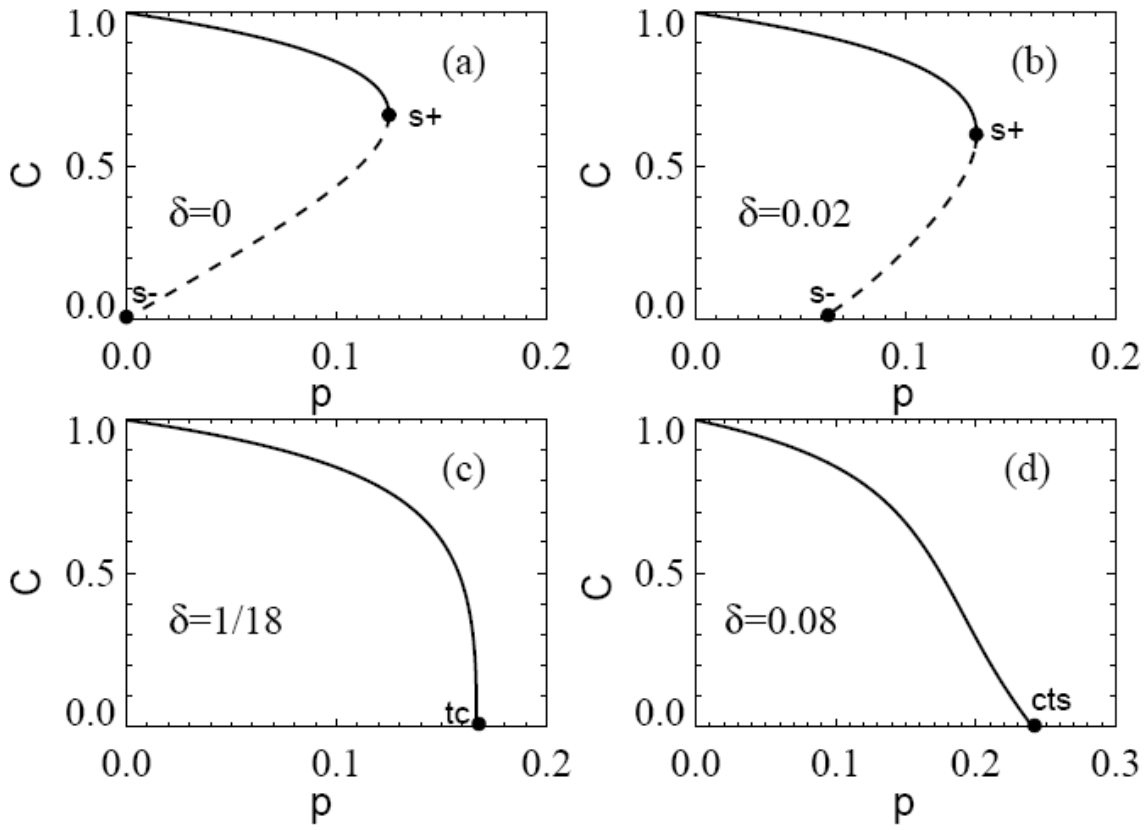

Figure 13: Pair-approximation prediction for variation of steady-state C(p) with p in the QCP+MCP with h=0: (a) $\delta=0$; (b) $0 < \delta < \delta_{tc}$; (c) $\delta = \delta_{tc} = 1/18$; (d) $\delta > \delta_{tc}$. The notation s+ and s- indicates upper and lower spinodals, respectively; tc indicates the tricritical point, and cts the continuous transition.

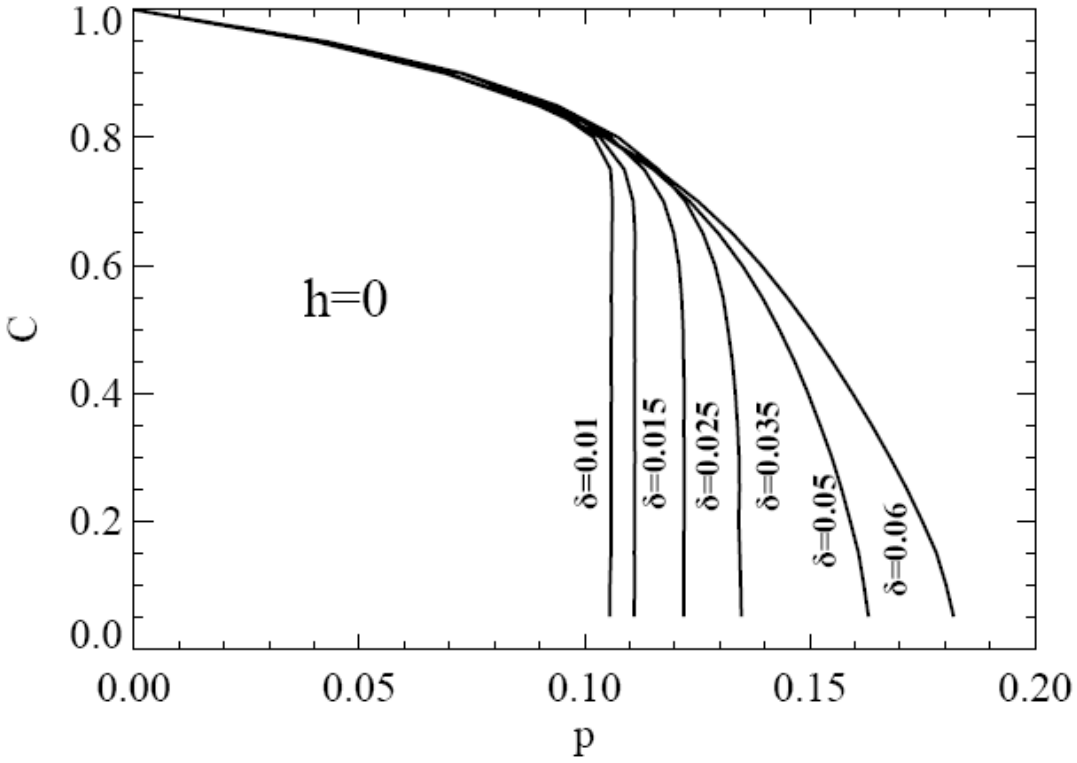

Figure 14: CC simulation results for steady-state behavior in the QCP+MCP with h=0 for various δ. From this data, we estimate that $\delta_{ct} \approx 0.026\text{-}0.028$.

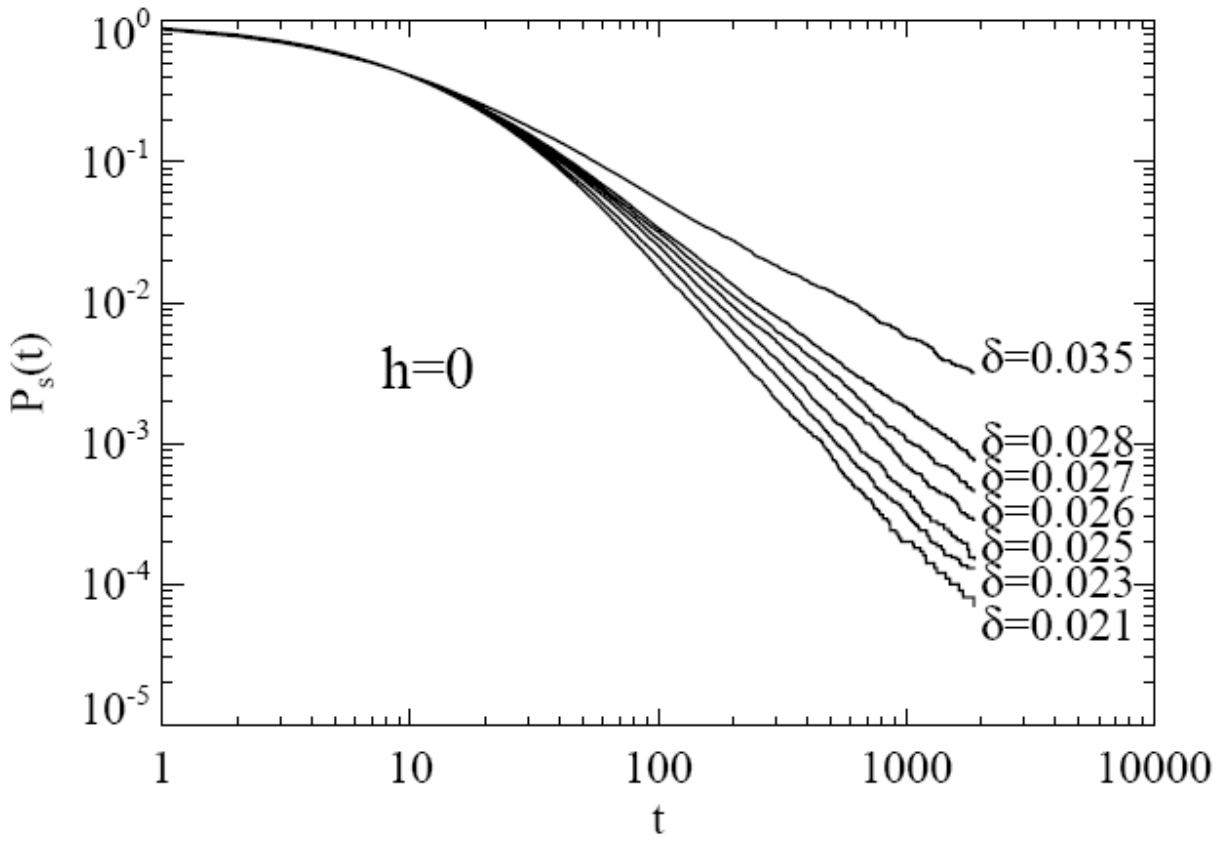

Figure 15: Epidemic analysis for the QCP+MCP with h=0. Survival probability, $P_s(t)$, versus time, t, for a single occupied site embedded in a vacuum state for various δ from 0.021 to 0.035, and choosing $p = p_{tr}(\delta)$. For $\delta_{ct} \approx 0.026$-$0.028$, one obtains $\zeta_{tc} = 1$